FULL PAPER

Ultrasound Contrast Agents

ADVANCED
FUNCTIONAL
MATERIALS

www.afm-journal.de

Thickness and Sphericity Control of Hollow Hard Silica Shells through Iron (III) Doping: Low Threshold Ultrasound Contrast Agents

Ching-Hsin Huang, James Wang, Jian Yang, Juan Pablo Oviedo, Seungjin Nam, William C. Trogler, Sarah L. Blair, Moon J. Kim, and Andrew C. Kummel*

Silica particles are convenient ultrasound imaging contrast agents because of their long imaging time and ease of modification; however, they require a relatively high insonation power for imaging and have low biodegradability. In this study, 2 µm ultrathin asymmetric hollow silica particles doped with iron (III) (Fe(III)-SiO$_2$) are synthesized to produce biodegradable hard shelled particles with a low acoustic power threshold comparable with commercial soft microbubble contrast agents (Definity) yet with much longer in vivo ultrasound imaging time. Furthermore, high intensity focused ultrasound ablation enhancement with these particles shows a 2.5-fold higher temperature elevation than with Definity at the same applied power. The low power visualization improves utilization of the silica shells as an adjuvant in localized immunotherapy. The data are consistent with asymmetric engineering of hard particle properties that improve functionality of hard versus soft particles.

1. Introduction

Ultrasound contrast agents are used to enhance image contrast and improve diagnostic and therapeutic functionality for drug delivery, tumor detection-characterization, and image-guided surgeries.[1–4] Among ultrasound contrast agents, microbubbles encapsulated by surfactants, lipids, and polymers are the most common.[5–7] However, conventional microbubbles and other soft-shelled structures suffer from rapid clearance from the injection site, short in vivo imaging lifetimes, large

bubble size variance, and complex surface modification procedures.[8–10] Therefore, hard particles made with silica are being studied as alternative contrast agents for ultrasound imaging because of their long shelf life, persistent imaging properties, high thermal stability, chemical stability, and low toxicity.[11–13]

In addition to ultrasound image contrast enhancement, several contrast agents have been reported to augment high intensity focused ultrasound (HIFU) therapy. HIFU therapy induces tissue necrosis through energy conversion of ultrasound energy to regional hyperthermia, and it has gained interest for tumor ablation applications.[14] Microbubbles enhance tumor ablation during HIFU therapy;[15–17] however, the short in vivo lifetime of their soft shells limits this application. Hard silica shells are long lived in tissue and even under insonation and, therefore, may offer better potential as HIFU therapy enhancers.[18,19]

Despite the advantages, rigid silica shells still require higher insonation power to fracture, which releases gas in situ and produces signal contrast comparable to soft shell particles. Since insonation energy deposited in tissue significantly attenuates with increasing penetration depth, for deeper tissue imaging, low power threshold imaging for hard silica shells is still required. Liberman et al. demonstrated that substitution of a fraction of the initial silica shell precursors with organically modified silanes produced thinner nanoshells. These thinner shells decreased ultrasound mechanical index (MI) imaging thresholds compared to the control nanoshells synthesized with only tetramethyl orthosilicates (TMOSs).[20]

In the present study, it is shown that in addition to substitution of the initial silica precursor with phenyl precursors,[20] the iron doping further alters the shell thickness and structural morphology. With 3.5% iron doping (corresponding to 0.010% w/v), 2 µm ultrathin iron (III) doped particles with irregular particle subpopulations were synthesized and demonstrated a 83% lower threshold for ultrasound imaging than non-iron doped particles. The power threshold of these asymmetric 2 µm ultrathin iron (III) doped silica hard particles is similar to that of soft shell commercial particles, which have much shorter imaging lifetimes.[10] The 2 µm ultrathin

C.-H. Huang, J. Wang, Dr. J. Yang, Prof. W. C. Trogler, Prof. A. C. Kummel
Department of Chemistry and Biochemistry
University of California, San Diego
9500 Gilman Drive, La Jolla, CA 92093, USA
E-mail: akummel@ucsd.edu
Dr. J. P. Oviedo, S. Nam, Prof. M. J. Kim
Department of Materials Science and Engineering
University of Texas at Dallas
Richardson, 800 W Campbell Rd, Richardson, TX 75080, USA
Dr. S. L. Blair
Moores Cancer Center
3855 Health Sciences Drive, La Jolla, CA 92093, USA

1900893 (1 of 9)

Table 1. The starting concentration of iron precursor of Fe(III)-SiO$_2$ shells and the final Fe atomic % and shell thickness.

Iron ethoxide starting concentration (% in w/v)	Fe(III) atomic % (by EDX)	Shell thickness [nm]	Fe(III)-SiO$_2$ sample[a]
0.020%	6.8 ± 2.9	21.1 ± 5.6	Thick shells
0.015%	5.7 ± 1.7	6.2 ± 2.3	Medium-thickness shells
0.010%	3.5 ± 1.0	2.7 ± 1.5	Ultrathin shells
0.005%	1.1 ± 0.5	–	–

[a]Iron (III) used in sample name "Fe(III)-SiO$_2$" refers to doping agent, iron (III) ethoxide.

Fe(III)-SiO$_2$ shells also exhibited a larger temperature rise during HIFU insonation compared to thicker shells or commercial microbubbles. These new ultrathin asymmetric Fe(III)-SiO$_2$ shells have the ability to amplify the immune response and potentially to be utilized as an adjuvant in localized immunotherapy which can be readily visualized by ultrasound imaging. In vitro cytokines analysis for the asymmetric 2 μm ultrathin silica shells in contact with RAW264.7 macrophages plus lipopolysaccharide (LPS), demonstrated a 40-fold increase in interleukin 1β (IL-1β) production compared to RAW264.7 macrophages plus LPS alone. The imaging, HIFU, and immune response results showed that engineering asymmetry opens a new dimension for tuning the properties of ultrasound active nanoparticles.

2. Results and Discussion

2.1. Iron (III) Doping Modulates Shell Thickness

Iron (III) doped silica shells with a diameter of 2 μm were synthesized with varying iron (III) doping concentrations

(**Table 1**). Transmission electron microscope (TEM) and scanning electron microscopy (SEM) images in **Figure 1** and Figure S1 in the Supporting Information show that the 2 μm iron doped silica shells (0.010%, 0.015%, and 0.020% of iron (III) ethoxide-concentrations are shown in weight/volume percentages) formed intact spherical structures. When iron (III) doping was reduced less than 0.010%, shell synthesis was not viable (Figure S1, Supporting Information). Based on energy-dispersive X-ray spectroscopy (EDX) analysis in Table 1, 0.01%, 0.015%, and 0.02% of Fe(OEt)$_3$ doping percent yielded 3.5 ± 1.0, 5.7 ± 1.7, and 6.8 ± 2.9 Fe (III) atomic % in final products, respectively.

The effect of iron (III) content on shell thickness and structure were quantified using TEM and imageJ software. Thickness was defined as the dense layer of the shells as previously described.[20] Figure 1 and Table 1 validated that iron (III) content controls shell thickness for a given silica precursor. The failure of shell formation with 0.005% iron (III) doping is consistent with insufficient iron (III) needed for shell strengthening (Figures S1–S3, Supporting Information). The formulations synthesized with 0.01% of iron (III) ethoxide have a markedly thinner shell thickness when compared to formulations with a higher iron (III) content, and thus were denoted as 2 μm ultrathin Fe(III)-SiO$_2$ shells (2.7 nm vs 21.1 nm thickness, respectively). Particles with 0.01% of iron (III) ethoxide will be referred to as ultrathin, particles with 0.015% of iron (III) ethoxide will be referred to as medium thickness, and particles with 0.02% of iron (III) ethoxide will be referred to as thick shell particles. X-ray photoelectron spectroscopy (XPS) spectra in Figure S4 in the Supporting Information indicated the iron is in its oxidized state.
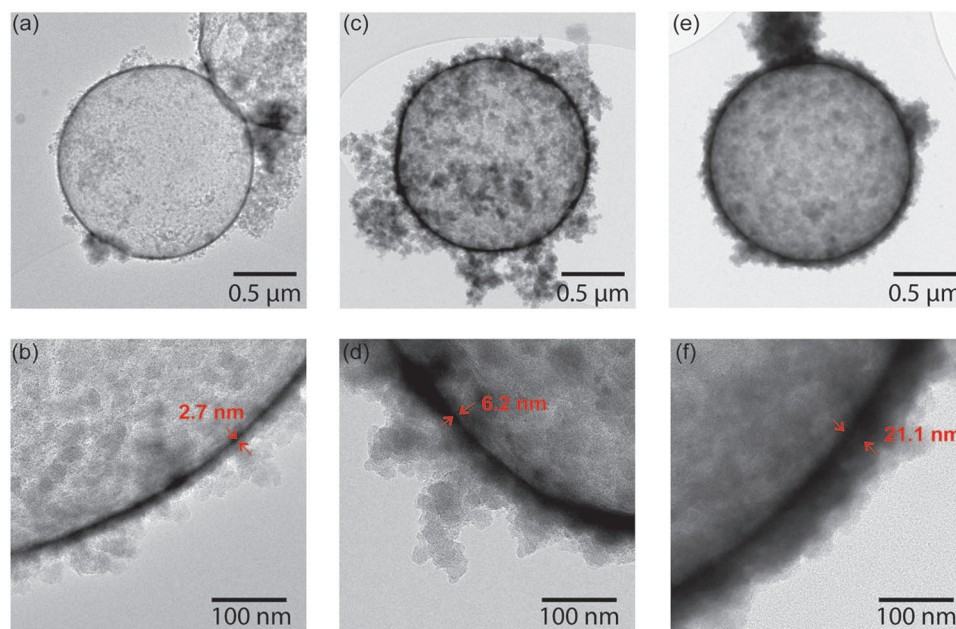

Figure 1. TEM images of iron (III) doped silica hollow shells. a,b) ultrathin, c,d) medium-thickness, and e,f) thick iron (III) doped silica shells.
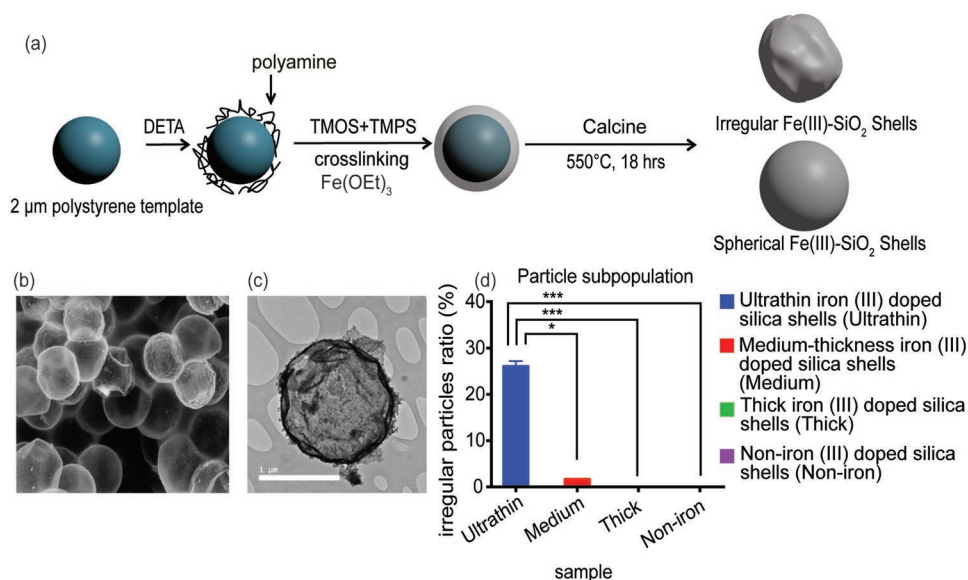
**ADVANCED
SCIENCE NEWS**
www.advancedsciencenews.com

**ADVANCED
FUNCTIONAL
MATERIALS**
www.afm-journal.de

Figure 2. Irregular particle subpopulation from ultrathin iron (III) doped silica shells. a) Synthesis of ultrathin shells with a large subpopulation of irregular shells. b) Representative SEM image of 2 µm Fe(III)-SiO$_2$ ultrathin shells containing spherical and irregular particle subpopulations. c) Representative TEM image of single irregular 2 µm Fe(III)-SiO$_2$ ultrathin shell. d) Irregular particle ratios in ultrathin Fe(III)-SiO$_2$ particles, medium-thickness Fe(III)-SiO$_2$ particles, thick Fe(III)-SiO$_2$ particles and non-iron (III) doped SiO$_2$ particles (Data were analyzed for fraction of irregular using Kruskal–Wallis test. P-values are as follows: *$P \leq 0.05$, **$P \leq 0.01$, ***$P \leq 0.001$).

2.2. Irregular Shells Formed by Low Iron (III) Doping

A correlation between iron (III) doping and particle sphericity was observed after examining more than 100 randomly obtained microscopy images for each sample. While only a 1.7% ± 1.7% irregular particle subpopulation was found in the medium-thickness Fe(III)-SiO$_2$ shells (0.015% w/v formula), a 26% ± 3% irregular particle subpopulation was observed in the ultrathin Fe(III)-SiO$_2$ shells. Irregular particles were not observed for either high iron (III) doped silica shells (0.020% w/v formula) nor non-iron (III) doped silica shells (**Figure 2**). Since iron (III) doping lower than 0.005% w/v could not produce an intact sphere structure under the synthetic conditions, 0.010% w/v of iron (III) doping was the optimal concentration for obtaining a significant fraction of irregular shells.

Previous studies show that a particle's shape is a critical factor in mechanical strength, and that the structural heterogenicity of the irregular particles can cause discrete local stresses.[21–23] For the 26% irregularly shaped subpopulation in the ultrathin particles, it is expected they will exhibit lower shell strength, fracture more easily, and, therefore, enhance the ultrasound imaging performance at lower insonation powers. Among the ultrathin Fe(III)-SiO$_2$ particles, nanoscale deep surface inclusions were also found in some particles as shown in Figure S5 in the Supporting Information, which implies that there may be more structural defects in the ultrathin shells that are not visible in TEM.

2.3. Low Ultrasound Imaging Threshold for New Ultrathin Fe(III)-SiO$_2$ Shells

To verify that sphericity and shell thickness of iron (III) doped silica shells control ultrasound performance, shells were filled with perfluoropentane (PFP) gas and imaged with ultrasonography. The ultrasound sensitivity of the particles was quantified using contrast pulse sequencing (CPS); CPS extracts nonlinear signals to produce images,[21] and the CPS signals (Figure S6, Supporting Information) correspond to echo decorrelation events. According to the CPS images shown in Figure S6 in the Supporting Information, 2 µm diameter thick and ultrathin shells began generating signals at MI = 0.66 and MI = 0.11, respectively. The average intensity of pixels in CPS images was referred to brightness in this study. When the MI started at 0.06, the signal was due to background noise which was ≈50 a.u. (**Figure 3**a–c). As the MI increased, the intensity of pixels in CPS images increased far above the background noise. As shown in Figure 3a, the 2 µm ultrathin shells demonstrated a much lower power insonation threshold for CPS brightness (at frame 55; MI = 0.11) than the thick shells (at frame 150; MI = 0.66). The differences in brightness profiles are attributed to the thick shells providing a more robust structure so that there are fewer shells fractured at low MI. In Figure 3a, as the MI was increased, the ultrathin shells generated two plateaus at MI = 0.9 and 1.9. For the first plateau, it was hypothesized that the ultrasound waves at low insonation power (MI = 0.2–0.9) interacted with the irregular shells that have a weaker structure, breaking the irregular shells to release gas and create more nonlinear events. It was hypothesized that the second plateau represents the 2 µm ultrathin shells with a normal spherical structure fracturing to release PFP gas at higher insonation powers and enhancing the output ultrasound signals (MI = 1.0–1.9).

The effect of shell thickness on threshold power for CPS was quantified using a new metric. The threshold for CPS brightness was defined as 20% of the maximum brightness at MI = 1.9. The power threshold of ultrathin, medium-thickness, and thick shells occurred at MIs of 0.2, 1.0, and 0.97, respectively (Figure 3d).
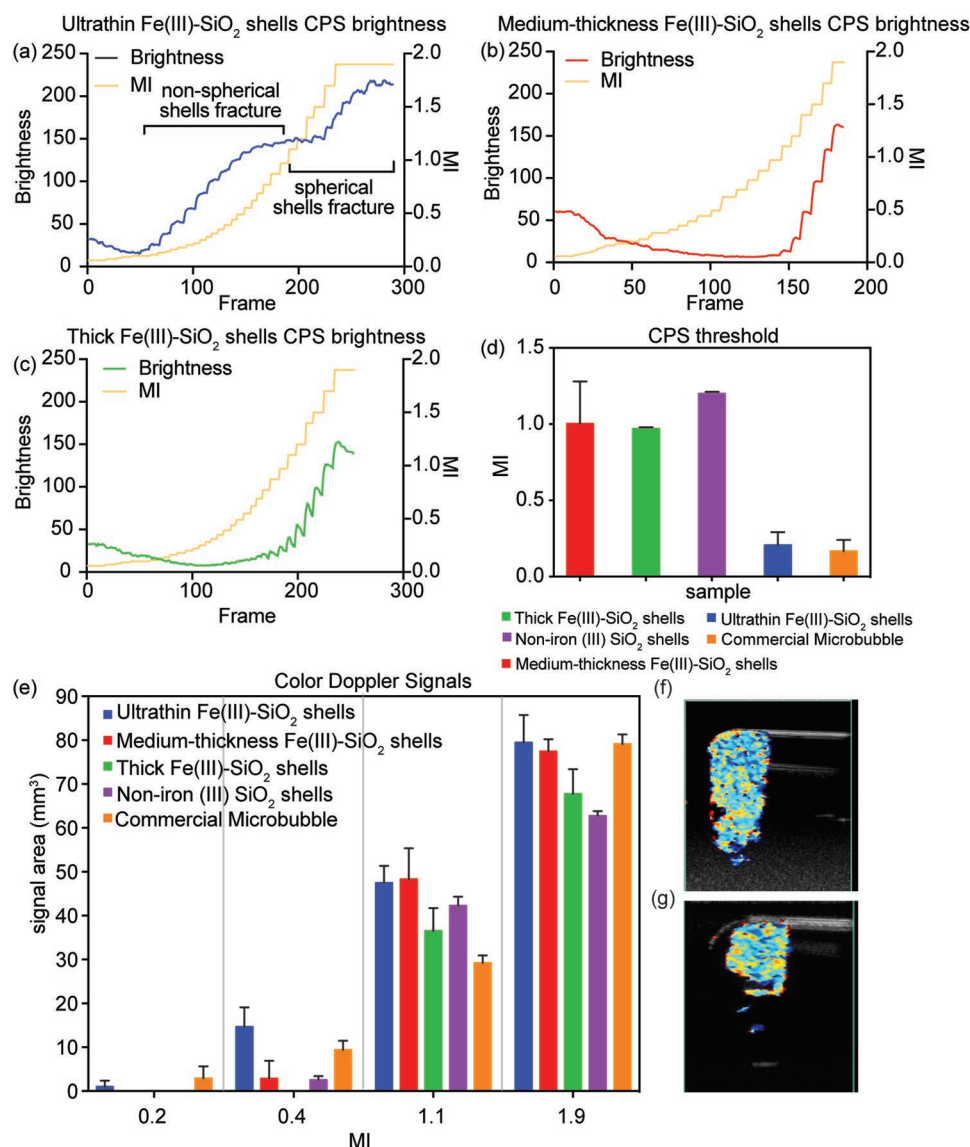
Figure 3. CPS and color Doppler ultrasound imaging of PFP-filled iron (III) doped silica shells, non-iron (III) doped silica shells and microbubbles. a–c) CPS brightness of iron (III) doped silica shells over frames from MI = 0.06 to MI = 1.9. a) Ultrathin Fe(III)-SiO$_2$ 2 µm shells, b) medium-thickness Fe(III)-SiO$_2$ 2 µm shells, and c) thick Fe(III)-SiO$_2$ 2 µm shells. d) CPS thresholds of non-iron (III) doped 2 µm silica shells, commercial microbubbles (Definity), and thick, medium-thickness, and ultrathin Fe(III)-SiO$_2$ shells. e) Color Doppler imaging of 2 µm shells with thick, medium-thick, ultrathin thickness, compared to non-iron (III) doped shells and microbubbles (Definity). f) Image of color Doppler ultrasound of ultrathin Fe(III)-SiO$_2$ shells at MI = 1.9. g) Image of color Doppler ultrasound of thick Fe(III)-SiO$_2$ shells at MI = 1.9.

By reducing the iron (III) doping and reducing corresponding shell thickness and symmetry, the threshold of CPS imaging of ultrathin shells decreased by 83% (p-value = 3.00×10^{-5}) compared to the thick symmetric non-iron (III) doped shells.

A commercial contrast agent (Definity) was used for comparing the ultrasound performance of fluorocarbon-filled soft shells with the PFP-filled ultrathin Fe(III)-SiO$_2$ hard shells. Definity is a clinically used microbubble emulsion filled with octafluoropropane gas that has an extremely low CPS threshold, but at the same time it has a large size distribution and short imaging lifetime; in vivo studies showed that microbubbles can only be imaged for few minutes.[22]

Definity was tested at equivalent gas volume concentration as silica shells. The ultrathin iron (III) doped hard shells and commercial microbubbles have no difference in imaging thresholds (p-value = 0.88) and both demonstrated low threshold mean (MI = 0.20 and 0.16, respectively) as shown in Figure 3d. These results indicate the feasibility of microbubble alternative by rigid ultrathin iron (III) doped silica shells that provide a longer imaging usage time.

Similar to CPS imaging, the enhancement of color Doppler imaging by PFP-filled Fe(III)-SiO$_2$ hard shells were tested in vitro. Appearance of the first signal of the color Doppler image is presented in Figure 3e. Consistent with the CPS results, the
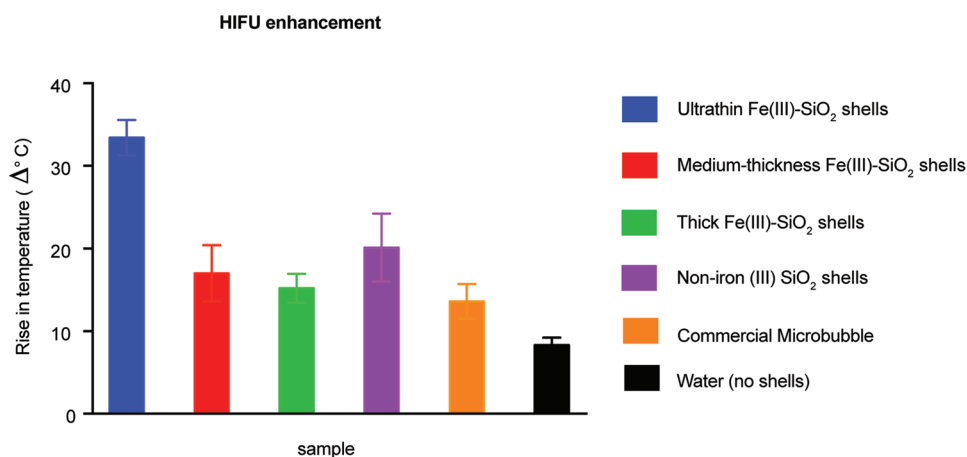
Figure 4. HIFU response of iron (III) doped silica shells, non-iron (III) doped silica shells, commercial microbubbles, and absence of shells (pure water). 0.4 mg mL^{-1} silica shells or Definity microbubbles at the same gas volume were applied HIFU (100 Watts) at 100% duty cycle for 10 s.

ultrathin asymmetric shells showed a lower threshold compared to thick shells. Signals from the 2 µm ultrathin shells and microbubbles (Definity) both appeared at MI = 0.2 with similar signals, while that of the thick shells first appeared at MI = 1.1. At modest insonation power (MI = 0.4–1.1), ultrathin and medium thickness iron (III) doped shells showed a much stronger signal compared to Definity (Figure 3f,g).

2.4. HIFU Enhancement by Ultrathin Fe(III)-SiO$_2$ Shells

Several commercial microbubble contrast agents such as Levovist, Optison, and Definity have been studied to enhance HIFU treatment.[23,24] In the present study, the enhancement of HIFU by particles was characterized in vitro by comparing the temperature rise of a solution of silica shells, commercial microbubbles with same gas volume, and pure water. In **Figure 4**, ultrathin Fe(III)-SiO$_2$ shells demonstrated a 33.4 °C temperature rise from 23.1 to 56.5 °C after applying 100 W 100% duty cycle HIFU for 10 s. Conversely, thick and medium thickness Fe(III)-SiO$_2$ shells only increased the temperature by ≈15.2 °C from 23.6 to 38.8 °C, and 17.0 °C from 23.4 to 40.4 °C, respectively. In water without added particles, the temperature only increased by 8.3 °C under HIFU exposure, which is approximately a quarter of temperature rise obtained by the ultrathin Fe(III)-SiO$_2$ shells. At the same applied HIFU power and the same gas volume concentration, commercial microbubbles (Definity) produced only 13.6 °C of temperature rise (from 20.5 to 34.1 °C). This is a 2.5-fold smaller temperature rise compared to ultrathin Fe(III)-SiO$_2$ hard shells. The data confirms and quantifies the HIFU enhancement effects achieved by the ultrathin hard microshells ultrasound contrast agent.

2.5. Biodegradability

Pohaku-Mitchell et al. demonstrated that by doping iron (III) into nanometer-sized silica shells at 6 at% Fe, the silica particles became biodegradable through an iron (III)-chelating pathway via transferrin after 17 d incubation with human serum.[25] To

test the in vitro biodegradability of the new ultrathin shells, 2 µm non-iron (III) doped silica shells, thick Fe(III)-SiO$_2$ shells (6.8 at% Fe), and ultrathin Fe(III)-SiO$_2$ shells (3.5 at% Fe) were immersed in human serum for 24 d. The morphology of the silica shells was monitored to determine the progress of biodegradation (Figures S7 and S8, Supporting Information). As shown in Figure S8 in the Supporting Information, on the 8th day, both ultrathin and thick Fe(III)-SiO$_2$ shells began merging into irregular solid clusters while the nanosized Fe(III)-SiO$_2$ particles remained mostly intact on day 10 in previous studies.[25] On day 24, ultrathin Fe(III)-SiO$_2$ samples predominantly disappeared, whereas thick Fe(III)-SiO$_2$ samples remained partially intact. The non-iron (III) doped silica shells remained mainly intact in serum over the course of 24 d. It is hypothesized that thinner shells are easier to degrade despite the decreased amount of iron (III) doping. Only 3.5 at% of iron (III) doping is sufficient to convert nonbiodegradable silica matrix to biodegradable shells while in the literature 6% of iron (III) doping gave a much slower biodegradation profile due to the much thicker shells.[25]

2.6. In Vivo Imaging Threshold and Persistence of Fe(III)-SiO$_2$ Shells

The iron (III) doped silica shells were tested for use as an intraoperative, low threshold color Doppler tissue marker in vivo. Imaging was performed at 7 MHz, the previously determined optimal frequency. 0.4 mg of ultrathin or thick Fe(III)-SiO$_2$ shell solutions were intramuscularly injected into mice, and insonation power was increased from MI = 0.06 to MI = 1.9. The color Doppler signal was monitored over different insonation powers to assess the in vivo imaging enhancement by the 2 µm shells. **Figure 5**a shows that thick shells began to show the first signal at MI = 1.1 and persisted to MI = 1.9, yet the signals remained faint throughout the MI range. In contrast, ultrathin shells produced the first signal at MI = 0.37; a threshold value over 3 × lower than that of the thicker shells. As the MI increased, the color Doppler signals
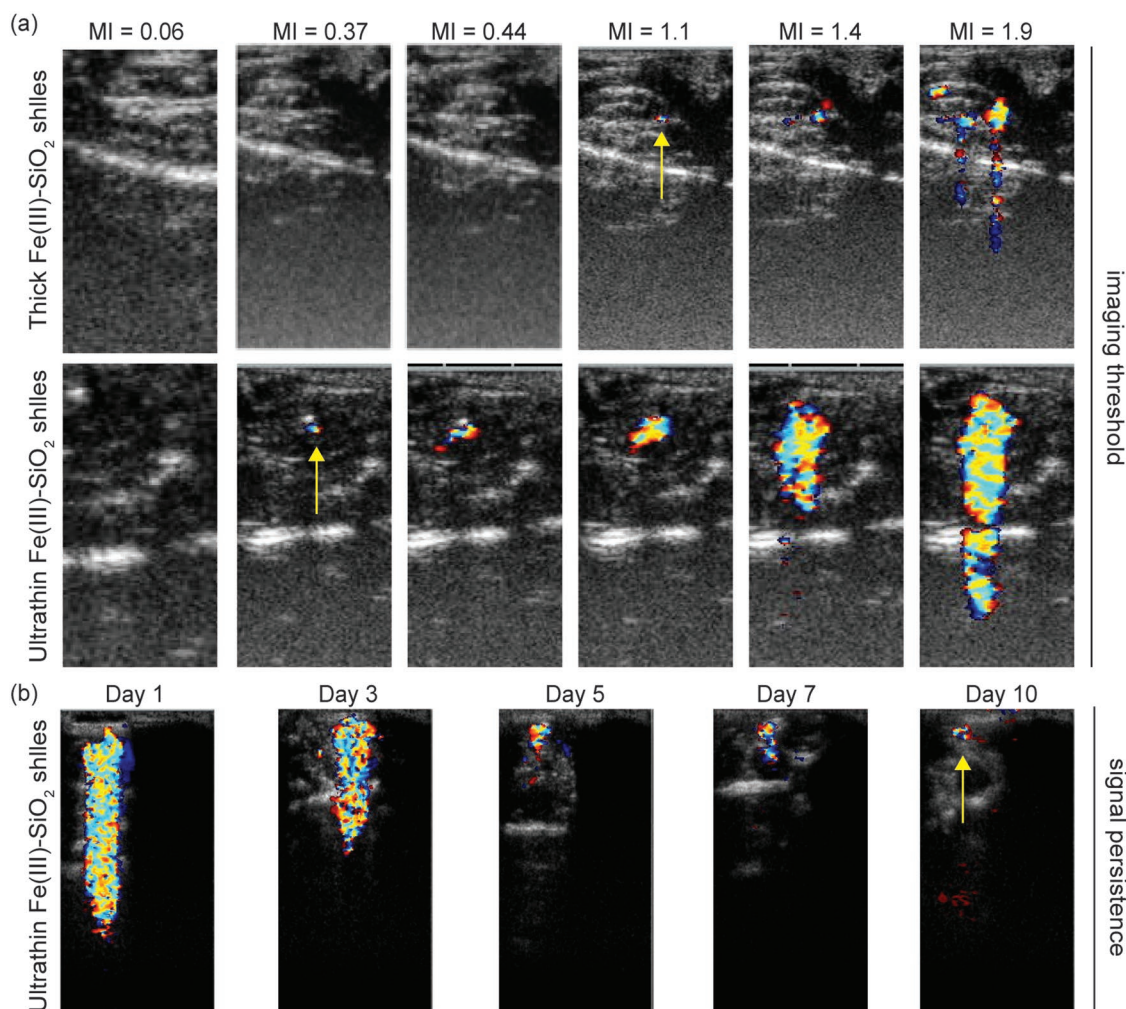
**ADVANCED
SCIENCE NEWS**
www.advancedsciencenews.com

**ADVANCED
FUNCTIONAL
MATERIALS**
www.afm-journal.de

Figure 5. In vivo color Doppler ultrasound images of 2 µm Fe(III)-SiO$_2$ shells filled with PFP gas. a) Thresholds of thick Fe(III)-SiO$_2$ shells and ultrathin Fe(III)-SiO$_2$ shells. Shells were injected into mice intramuscularly and imaged with MIs from 0.06 to 1.9. b) Signal persistence of ultrathin Fe(III)-SiO$_2$ shells. Shells were injected into mice intramuscularly and imaged over the course of 10 d at MI = 1.9.

became stronger until MI = 1.9, by which point the signal surpassed that of thicker shells. With the improved performance of in vivo color Doppler imaging and HIFU enhancement, these new ultrathin asymmetric iron (III) doped silica hard shells offer added safety in applications of image-guided HIFU tumor ablation, by providing HIFU enhancement at reduced power levels.

To explore the potential utilization as long term ultrasound biomarkers, these ultrathin asymmetric Fe(III)-SiO$_2$ shells were injected into mice flanks and imaged over 10 d at MI = 1.9 to assess the signal persistence. The commercially available microbubbles Definity could only be imaged within a few minutes after injection on the first day as reported previously.[10] The color Doppler of Definity could not be detected after 1 d. Conversely, the gas filled ultrathin 2 µm Fe(III)-SiO$_2$ shells could be detected for 10 d in vivo after the initial injection. The results shown in Figure 5b also indicated that the 2 µm ultrathin Fe(III)-SiO$_2$ shells remained stationary at the injected tissue and did not excavate from the injected tissue site. The in vivo imaging stability and the long retention time at the

injection site suggested the promising application for these ultrathin asymmetric shells to be used as tissue labeling agents.

2.6.1. 2 µm Ultrathin Fe(III)-SiO$_2$ Shells Can Be Used as an Immune Adjuvant

The aforementioned advantages for these new ultrathin asymmetric Fe(III)-SiO$_2$ shells, such as prolonged persistency and easy visualization, are important in promoting a mature immune response and designing immunotherapy strategies, respectively.[26] Since silica nanoparticles have been previously reported to be a strong immune adjuvant that amplify antibody production and elicit immunological protection response,[27] it is hypothesized that these new Fe(III)-SiO$_2$ 2 µm shells can also effectively activate immune response while being able to generate stable ultrasound signals for tracking the adjuvant location. To test their adjuvanticity, innate immune cells, macrophages RAW264.7, primed with LPS were incubated with shells and IL-1β in the supernatant was measured by

**ADVANCED
SCIENCE NEWS**

www.advancedsciencenews.com

**ADVANCED
FUNCTIONAL
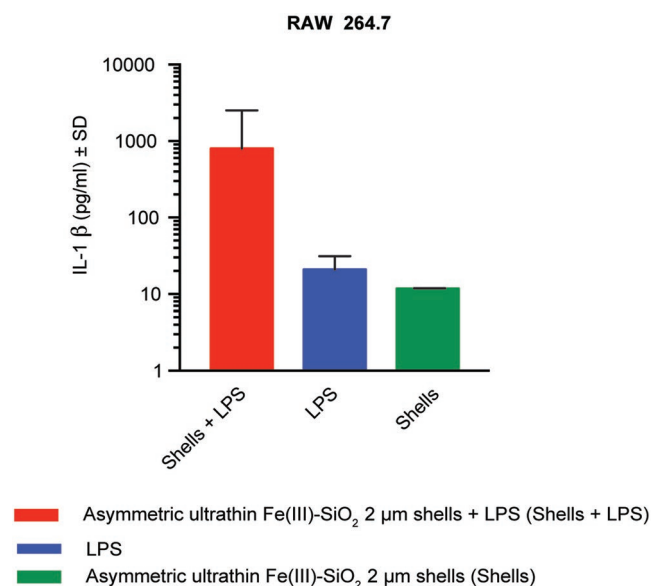MATERIALS**

www.afm-journal.de

Figure 6. In vitro adjuvanticity of ultrathin asymmetric Fe(III)-SiO₂ shells. 10^4 cells per well of RAW264.7 were incubated with iron (III) doped silica shells and/or LPS to determine the adjuvanticity of these new ultrathin asymmetric Fe(III)-SiO₂ shells.

enzyme-linked immunosorbent assay (ELISA) to assess the activation level of macrophages. IL-1β is able to enhance dendritic cells activation and T cells priming, stimulating an effective adaptive immune response.[28] As shown in **Figure 6**, these new ultrathin asymmetric Fe(III)-SiO₂ shells induced a 40-fold increase in IL-1β in cells primed with LPS compared to LPS alone. This result suggests that these new Fe(III)-SiO₂ shells have the ability to amplify the immunity, indicating the potential to be utilized as an adjuvant in immunotherapy with medical imaging capabilities.[29]

3. Conclusion

The extent of iron (III) doping can be used to modify the thickness and structural morphology of silica shells. The low iron (III) doping (0.010% w/v) not only generated thinner shells but also produced a 26% irregular particle subpopulation among the ultrathin hard shells. These new asymmetric ultrathin Fe(III)-SiO₂ hard shells demonstrated similar performance to the commercial soft particle contrast agent, Definity, which suffers from short imaging duration. HIFU sensitization tests showed that asymmetric ultrathin 2 µm Fe(III)-SiO₂ shells induced a greater HIFU response compared to symmetric thicker shells and microbubbles. The persistency experiments demonstrated that these new Fe(III)-SiO₂ shells can be imaged in vivo for a much longer time compared to commercial microbubbles. The enhanced performance of these new Fe(III)-SiO₂ shells originates from two structural variances; the thinner shells and the irregular particles are mechanically weaker. It has been demonstrated that a new variable, asymmetry, may be introduced into hard shelled contrast agents in order to tune their structural integrity. A more fragile structure may expand their applications; for example, these new ultrathin asymmetric
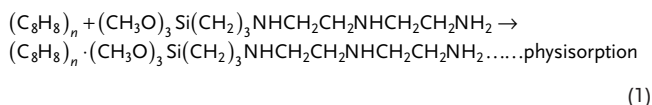
Fe(III)-SiO₂ shells capable of amplifying immune response can be used as a local immunotherapy with effective ultrasound visualization.

4. Experimental Section

Materials: TMOS, trimethyloxyphenylsilane (TMPS), and N1-(3-trimethoxysilylpropyl) diethylenetriamine (DETA) were purchased from Sigma-Aldrich (St. Louis, MO) and the polystyrene beads were purchased from PolySciences Inc. (Warrington, PA). Iron (III) ethoxide was purchased from Gelest Inc. (Moorisville, PA). Heat inactivated human serum was purchased from Gemini Bio-Products Inc (West Sacamento, CA). Ultrasound images were acquired with use of a Seimens Sequoia 512 (Mountainview, CA), and an Acuson 15L8 imaging transducer. The H-102 single element transducer used in HIFU experiments was acquired from Sonic Concepts Inc (Bothell, WA). Software programs used for data analysis include Matlab (Natick, MA), ImageJ, Microsoft Excel (Redomond, WA), GraphPad Prism (La Jolla, CA), and OsiriX (Bernex, Switzerland).

Synthesis of Silica Shells: A 0.2% DETA solution was prepared in ethanol solvent and vortexed slightly to mix. Subsequently, 100 mL of ethanol, 8 mL of 0.2% DETA solution, and 5 mL of 2 µm polystyrene beads were vortex-mixed for an hour to produce cationic polystyrene beads. 270 µL of TMOS was added and vortex mixed for an additional 7.5 h to generate robust non-iron (III) doped 2 µm silica shells. Trimethoxyboron was also added to the sol gel synthesis to enhance the shell structure as previously described.[30] To generate thinner shells, the silica precursor amount was reduced to 70 mol% using a TMOS/TMPS mixture (1:1 molar ratio). The silica precursor solution was added into the cationic beads reaction mixture and mixed for an additional 5 h. This reduced amount of silica precursor did not allow shell formation after calcination. However, by incorporating iron (III) into the silica network to strengthen the shells, an intact thin shell structure was obtained. The detailed synthesis process is as follows for four iron (III) doping levels. 1000, 750, 500, or 250 µL of the 20 mg mL⁻¹ iron (III) ethoxide solution were added into the DETA/polystyrene beads mixture together with the silica precursor solution, and vortex mixed for 5 h, to produce iron (III) doped silica shells. Brown core–shell Fe(III)-SiO₂ particles were collected by centrifugation at 3500 rpm for 5 min, and washed twice with 15 mL of ethanol. The core–shell particles were calcined in air in a muffle furnace, starting from room temperature and heating at 1.5 °C per minute to 550 °C to yield ≈20 mg of the rigid hollow particles. Reactions are shown as below and Figure S9 in the Supporting Information

Step (1): DETA was added into polystyrene beads mixture in ethanol to assist templating reaction

$$(C_8H_8)_n + (CH_3O)_3 Si(CH_2)_3 NHCH_2CH_2NHCH_2CH_2NH_2 \rightarrow$$
$$(C_8H_8)_n \cdot (CH_3O)_3 Si(CH_2)_3 NHCH_2CH_2NHCH_2CH_2NH_2 \ldots\ldots physisorption$$

$$(1)$$

Step (2): TMOS, TMPS, and iron (III) ethoxide were added into polyamine-modified polystyrene beads mixture. TMOS and TMPS reacted with H₂O presented in the solution and started hydrolysis and iron (III) was incorporated into silica network, cationic protonated DETA helped attract anionic deprotonated sol hydrolysis products for templating on the polystyrene bead surface

$$Si(OR)_4 + H_2O \rightarrow HO - Si(OR)_3 + R - OH \qquad (2)$$
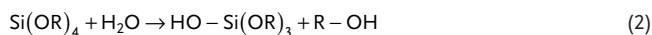
Step (3): Spin down the iron(III)/silica-polystyrene core–shells. Calcine and obtain hollow iron(III) doped silica shells.

The 70 mol% of TMOS/TMPS mixture was a previously determined to be the optimized silica precursor concentration to generate thin silica shells. It was observed that a lower amount of initial silica precursor concentration, even with addition of iron ethoxide to strength the shells or with addition of increased DETA to attract more silicic acid to the

polystyrene bead template surface, would fail to robustly generate intact shell formation (Figure S2, Supporting Information).

Characterization of Particles: The iron (III) doped silica shell particles were imaged in a JEOL 2100F TEM operating at 200 kV. TEM samples were prepared by drop-casting the shells (diluted in ethanol) on lacey carbon coated copper TEM grids. Energy filtered imaging TEM through a Gatan imaging filter (Tridiem) was used to investigate the elemental distribution in the sample. In addition, the shell thickness was measured from high-magnification TEM images in ImageJ software.

Biodegradability: Iron (III) doped or non-iron (III) doped 2 µm silica shells were dispersed at 1 mg mL^{-1} concentration in heat inactivated human serum. The samples were vortex mixed to suspend the particles and incubated at 37 °C in a temperature-controlled water bath. The samples were vortexed every 24 h. The human serum was replaced with fresh human serum every 4 d after centrifugation and samples were vortexed to resuspend the shells. Every 8 d, a pellet was isolated by centrifugation, washed twice with water, and calcined. SEM images and EDX analysis of the pellet at each time point were obtained to characterize the extent of biodegradation.

Ultrasound CPS and Color Doppler Imaging Characterization: The 2 µm shells were suspended in 1 mL of water at a concentration of 0.4 mg mL^{-1} in a pipette bulb. Microbubbles (Definity) with gas volumes equivalent to the shells were filled in a pipette bulb tube. The bulb was placed in a water bath with an ultrasound transducer placed perpendicularly. Ultrasound was applied at 7 MHz for both CPS imaging and color Doppler imaging from low to high insonation power, which is referred to as the MI values in the study.

High Intensity Focused Ultrasound: 100 µL of 4 mg mL^{-1} PFP-filled Fe(III)-SiO$_2$ shell/water suspension was mixed with 900 µL of water in a pipette bulb. Definity microbubbles at the same gas volume as occupied by the silica microshells were used for comparison. The bulb was placed in the focal region of the HIFU transducer. HIFU power of 100 W was applied at a 100% duty cycle for 10 s. The temperature rise for each sample was measured with a thermocouple.

In Vitro Studies: RAW264.7 cells (mouse macrophage cell line) were purchased from the American Type Culture Collection (Rockville, MD) and cultured in complete Dulbecco's modified Eagle's medium (DMEM) media (Gibco, Carlsbad, CA). Cells were plated at a concentration of 104 cells well^{-1} and primed with lipopolysaccharide at 100 ng mL^{-1} for 2 h before exposure to silica shells. IL-1β in the supernatant after 18 h incubation was measured by ELISA kit (Cat. No. DY401, R&D system, Minneapolis, MN).

In Vivo Studies: The C57BL/6 mice were purchased from the Jackson Laboratory (Bar Harbor, ME). 50 µL of 4 mg mL^{-1} shell/water suspension was intramuscularly injected into the flank of each mouse. Color Doppler images were acquired continuously as the MI was increased from 0.06 to the maximum clinically allowable MI of 1.9. The threshold is defined as the first signal generated in the color Doppler images as the MI is increased. For the signal persistence study, the images were taken daily at MI = 1.9 for 10 d. All animal procedures have been approved by the Institutional Animal Care and Use Committee at University of California, San Diego.

Supporting Information

Supporting Information is available from the Wiley Online Library or from the author.

Acknowledgements

Conflict of Interest

S.L.B's spouse is co-founder, CEO and has equity interest in Viewpoint Medical Inc. A.C.K. and W.C.T. are scientific advisors, scientific co-founders, and have an equity interest in Viewpoint Medical Inc. The terms of this arrangement have been reviewed and approved by the University of California, San Diego in accordance with its conflict of interest policies.

Keywords

[1] F. Kiessling, S. Fokong, J. Bzyl, W. Lederle, M. Palmowski, T. Lammers, *Adv. Drug Delivery Rev.* **2014**, *72*, 15.

[2] K. Ferrara, R. Pollard, M. Borden, *Annu. Rev. Biomed. Eng.* **2007**, *9*, 415.

[3] H. Uemura, F. Sano, A. Nomiya, T. Yamamoto, M. Nakamura, Y. Miyoshi, K. Miki, K. Noguchi, S. Egawa, Y. Homma, Y. Kubota, *World J. Urol.* **2013**, *31*, 1123.

[4] E. J. Halpern, *Rev. Urol.* **2006**, *8*, S29.

[5] S. Unnikrishnan, A. L. Klibanov, *Am. J. Roentgenol.* **2012**, *199*, 292.

[6] S. Sirsi, M. Borden, *Bubble Sci., Eng., Technol.* **2009**, *1*, 3.

[7] J.-M. Correas, L. Bridal, A. Lesavre, A. Méjean, M. Claudon, O. Hélénon, *Eur. Radiol.* **2001**, *11*, 1316.

[8] K. Sarkar, A. Katiyar, P. Jain, *Ultrasound Med. Biol.* **2009**, *35*, 1385.

[9] E. G. Schutt, D. H. Klein, R. M. Mattrey, J. G. Riess, *Angew. Chem., Int. Ed.* **2003**, *42*, 3218.

[10] A. Liberman, H. P. Martinez, C. N. Ta, C. V. Barback, R. F. Mattrey, Y. Kono, S. L. Blair, W. C. Trogler, A. C. Kummel, Z. Wu, *Biomaterials* **2012**, *33*, 5124.

[11] P.-L. Lin, R. J. Eckersley, E. A. H. Hall, *Adv. Mater.* **2009**, *21*, 3949.

[12] H. Hu, H. Zhou, J. Du, Z. Wang, L. An, H. Yang, F. Li, H. Wu, S. Yang, *J. Mater. Chem.* **2011**, *21*, 6576.

[13] N. Mendez, A. Liberman, J. Corbeil, C. Barback, R. Viveros, J. Wang, J. Wang-Rodriguez, S. L. Blair, R. Mattrey, D. Vera, W. Trogler, A. C. Kummel, *Nanomedicine* **2017**, *13*, 933.

[14] Y.-F. Zhou, *World J. Clin. Oncol.* **2011**, *2*, 8.

[15] Y. Zhou, Z. Wang, Y. Chen, H. Shen, Z. Luo, A. Li, Q. Wang, H. Ran, P. Li, W. Song, Z. Yang, H. Chen, Z. Wang, G. Lu, Y. Zheng, *Adv. Mater.* **2013**, *25*, 4123.

[16] N. Hamano, Y. Negishi, Y. Takatori, Y. Endo-Takahashi, R. Suzuki, K. Maruyama, T. Niidome, Y. Aramaki, *Biol. Pharm. Bull.* **2014**, *37*, 174.

[17] K. Kajiyama, K. Yoshinaka, S. Takagi, Y. Matsumoto, *Phys. Procedia* **2010**, *3*, 305.

[18] A. Liberman, Z. Wu, C. V Barback, R. D. Viveros, J. Wang, L. G. Ellies, R. F. Mattrey, W. C. Trogler, A. C. Kummel, S. L. Blair, *J. Surg. Res.* **2014**, *190*, 391.

[19] X. Wang, H. Chen, Y. Chen, M. Ma, K. Zhang, F. Li, Y. Zheng, D. Zeng, Q. Wang, J. Shi, *Adv. Mater.* **2012**, *24*, 785.

[20] A. Liberman, J. Wang, N. Lu, R. D. Viveros, C. A. Allen, R. F. Mattrey, S. L. Blair, W. C. Trogler, M. J. Kim, A. C. Kummel, *Adv. Funct. Mater.* **2015**, *25*, 4049.

[21] P. Phillips, E Gardner, P. Phillips, E. Gardner, *Eur. Radiol. Suppl.* **2004**, *14*, P4.

**ADVANCED
SCIENCE NEWS**

www.advancedsciencenews.com

**ADVANCED
FUNCTIONAL
MATERIALS**

www.afm-journal.de

[22] A. Liberman, H. Paul Martinez, C. N. Ta, C. V Barback, R. F. Mattrey, Y. Kono, S. L. Blair, W. C. Trogler, A. C. Kummel, Z. Wu, *Biomaterials* **2012**, *33*, 5124.

[23] Y.-S. Tung, H.-L. Liu, C.-C. Wu, K.-C. Ju, W.-S. Chen, W.-L. Lin, *Ultrasound Med. Biol.* **2006**, *32*, 1103.

[24] S.-I. Umemura, K.-I. Kawabata, K. Sasaki, *IEEE Trans. Ultrason., Ferroelectr. Freq. Control* **2005**, *52*, 1690.

[25] K. K. Pohaku Mitchell, A. Liberman, A. C. Kummel, W. C. Trogler, *J. Am. Chem. Soc.* **2012**, *134*, 13997.

[26] T. J. Moyer, A. C. Zmolek, D. J. Irvine, *J. Clin. Invest.* **2016**, *126*, 799.

[27] D. Skrastina, I. Petrovskis, I. Lieknina, J. Bogans, R. Renhofa, V. Ose, A. Dishlers, Y. Dekhtyar, P. Pumpens, *PLoS One* **2014**, *9*, e114006.

[28] L. Xin, Y. Li, L. Soong, *Infect. Immun.* **2007**, *75*, 5018.

[29] H. Hogenesch, *Front. Immunol.* **2012**, *3*, 406.

[30] H. P. Martinez, Y. Kono, S. L. Blair, S. Sandoval, J. Wang-Rodriguez, R. F. Mattrey, A. C. Kummel, W. C. Trogler, *MedChemComm* **2010**, *1*, 266.

1900893 (9 of 9)